Inorganic Chemistry

Article

pubs.acs.org/IC

Efficient Near-UV Emitters Based on Cationic Bis-Pincer Iridium(III) Carbene Complexes

Noviyan Darmawan,[†,‡,⊥] Cheng-Han Yang,[‡] Matteo Mauro,[‡,⊥] Matthieu Raynal,[§] Susanne Heun,[▽] Junyou Pan,[▽] Herwig Buchholz,[▽] Pierre Braunstein,[§] and Luisa De Cola*[,‡,⊥]

[†]NRW Graduate School of Chemistry, University of Münster, D-48149 Münster, Germany

[‡]Physikalisches Institut and CeNTech, University of Münster, Heisenbergstrasse 11, D-48149 Münster, Germany

[§]Laboratoire de Chimie de Coordination, Institut de Chimie, UMR 7177 CNRS, Université de Strasbourg, 4 rue Blaise Pascal, F-67081 Strasbourg Cedex, France

[▽]Merck KGaA, Frankfurter Strasse 250, D-64293 Darmstadt, Germany

Supporting Information

ABSTRACT: We report on the photophysical studies of two cationic near-UV emitters based on bis-pincer Ir(III) carbene complexes: $[Ir^{n\mathrm{Bu}}(C_{NHC}{}^{Me}CC_{NHC})_2]X$, where $Ir^{n\mathrm{Bu}}(C_{NHC}{}^{Me}CC_{NHC})$ is (4,6-dimethyl-1,3-phenylene-κC^2)bis(1-butylimidazol-2-ylidene) and X = I^- or PF_6^-). The compounds are highly emitting in deaerated CH_3CN solution with emission maxima at 384 and 406 nm, and photoluminescence quantum yields of 0.41 and 0.38, for $[Ir^{n\mathrm{Bu}}(C_{NHC}{}^{Me}CC_{NHC})_2]I$ and $Ir^{n\mathrm{Bu}}(C_{NHC}{}^{Me}CC_{NHC})_2]PF_6$, respectively. In order to gain deeper understandings into their structural and electronic features, as well as to ascertain the nature of the excited states involved into the electronic absorption processes, density functional theory (DFT) and time-dependent DFT (TD-DFT) calculations have been performed on the ground and excited states of the closely related complex $[Ir^{Me}(C_{NHC}{}^{Me}CC_{NHC})_2]^+$. In the solid state, an emission at low energy is observed (λ_{max} = 500 nm) for both complexes. However, the intensity of the emission at high energy versus the intensity of the new emission at low energy is dependent on the nature of counterions. The origin of this emission is not completely clear, but the experimental data point to the formation of trapping sites induced by aggregation processes involving the interaction between the cationic emitter and the counterion.

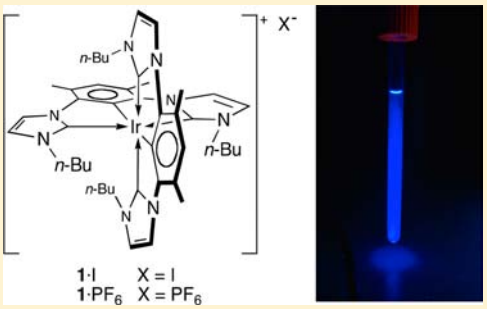

INTRODUCTION

Despite the rapid progress in the field of electroluminescent devices, efficient and stable deep-blue light-emitting transition-metal complexes remain elusive and still challenging.[1−3] In this respect, iridium *N*-heterocyclic carbene (NHC) complexes have been viewed as ideal triplet emitters, because of their high luminescence quantum yield, excellent color purity, and high stability imparted by the strong Ir−C_{NHC} bond.[4−10] Some examples of deep-blue neutral Ir carbene complexes have been reported, including the study of the influence of the ligand substitution on their photophysics and on the performance in organic light-emitting diodes (OLEDs).[5,7,9] However, charged Ir complexes emitting in the near-UV region (380−420 nm) suitable as emitting materials in light-emitting electrochemical cells (LEECs) have not been described so far in the literature, despite the fact that LEECs represent a promising alternative to OLEDs, because of their simpler architecture, and easier and lower-cost manufacturing.[11−14] Moreover, near-UV electroluminescent materials could find applications for medical purposes considering that many diseases are treated using UV light, where simple or even disposable devices are needed.[15−17]

Generally, one of the most promising strategies to have deep blue or near-UV emitting charged complexes lies in the choice of the chelating ligands, which must possess a very wide HOMO−LUMO gap and a very strong ligand field to avoid decomposition and low-lying states that can lead to non-radiative decays. Again, carbenes are a good choice, because of their high LUMO and deep HOMO and their strong coordination to the Ir(III) ion. Indeed, some examples of cationic heteroleptic complexes have been reported.[18−20] In such derivatives, the emission is mainly dominated by the choice of the noncarbene unit, which can be an ancillary, or the main ligand, as in the case of $[Ir(C\text{^}C_{NHC})_2(N\text{^}N)]^+$ and $[Ir(C\text{^}N)_2(N\text{^}C_{NHC})]^+$, respectively. This is due to the fact that, usually, the noncarbene ligands possess a smaller HOMO−LUMO energy gap and therefore determine the energy of the lowest-lying emitting state. We therefore decided to follow a different approach, employing a tridentate bis-carbene ligand, $C_{NHC}CC_{NHC}$, where $C_{NHC}CC_{NHC}$ is (1,3-phenylene-κC^2)bis(1-butylimidazol-2-ylidene), in order to obtain homoleptic bis-pincer Ir(III) complexes of general formula $[Ir(C_{NHC}CC_{NHC})_2]^+$. Luminescent Ir complexes based on terdentate ligands have attracted significant interest, because

Received: December 7, 2012
Published: September 9, 2013

of their unique properties compared to tris-bidentate Ir complexes. In fact, the coordination of only two ligands, possessing a tricoordination motif, leads to an increase in the rigidity, to the possibility of having a linear extension of the complex for the construction of rod-type systems, and to the formation of achiral compounds.[21−24] However, color tuning of these complexes in the blue region is still problematic,[25] and the photoluminescence efficiency are generally lower than their Ir bidentate analogues, because of the poorer bite angles and, therefore, weaker ligand-field strengths.[21] Thus, the introduction of a stronger unit such as $C_{NHC}CC_{NHC}$, as pincer ligand, to form a bis-terdentate system can be a potential solution to these drawbacks.

Even though $C_{NHC}CC_{NHC}$ ligands have been used to synthesize pincer-type complexes with several metal ions,[26−32] including the weak blue-emitting Pt complexes,[33,34] no report on the photophysics of pincer Ir carbene complexes appeared in the literature.[35−39] In addition, the synthesis of homoleptic bis-pincer Ir carbene complexes, $[Ir(C_{NHC}CC_{NHC})_2]^+$, has proven to be rather challenging, the very low reaction yields severely hampering the access to such complexes.[40] Recently, Braunstein and co-workers have shown that the presence of methyl groups in the C4 and C6 positions of the central phenyl ring and the use of an excess of triethylamine allowed an efficient access to the cationic bis−pincer $[Ir^{nBu}(C_{NHC}{}^{Me}CC_{NHC})_2]I$ complex, where $^{nBu}(C_{NHC}{}^{Me}CC_{NHC})$ is 4,6-(dimethyl-1,3-phenylene- κC^2)bis(1-butylimidazol-2-ylidene) (see Figure 1).[41] It is known that the addition of methyl

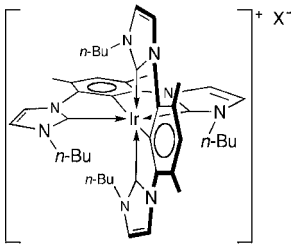

Figure 1. Schematic molecular structure of the cationic bis-pincer *n*-butyl carbene Ir(III) complexes.

groups in the central phenyl ring of the terdentate ligand, in the synthesis of Ir terdentate complexes, helps to prevent unwanted Ir binding modes from taking place.[23]

Herein, we have synthesized and crystallized $[Ir^{nBu}(C_{NHC}{}^{Me}CC_{NHC})_2]PF_6$ (**1**·PF_6) and studied its photophysical properties and those of the $[Ir^{nBu}(C_{NHC}{}^{Me}CC_{NHC})_2]I$ (**1**·I) analogue, in solution and in solid state. In solid state both the crystalline solids and the doped poly(methylmethacrylate), PMMA, thin films have been investigated. As a proof of principle, the first UV-emitting LEEC has been prepared and preliminary data are shown. Interestingly, the emission, within the electroluminescent device, retains its high energy profile.

RESULTS AND DISCUSSION

Synthesis and X-ray Structure. Complex **1**·I was prepared according to the method reported by Braunstein and co-workers.[41] Complex **1**·PF_6 was synthesized in quantitative yield by metathesis reaction of **1**·I with an excess of NH_4PF_6 in a mixture of CH_2Cl_2/CH_3OH at room temperature. Both complexes were obtained as off-white solids after purification by column chromatography and crystallization. Complexes **1**·I and **1**·PF_6 were fully characterized by high-resolution mass spectrometry, ^1H NMR spectroscopy, and elemental analysis (see the Experimental Section for details).

Single crystals of **1**·PF_6 suitable for X-ray determination were obtained via the slow diffusion of EtO_2 into a CH_2Cl_2 solution of **1**·PF_6 (see Table S1 in the Supporting Information). The crystal structure of **1**·I·CH_2Cl_2 has been described in a previous paper,[41] and it has been compared with the one obtained for the other counterion. The packing of desolvated crystal **1**·PF_6 has the $P2(1)/c$ space group, which is similar to the crystal of **1**·I·CH_2Cl_2. In general, molecular configuration and structural parameters of **1**·PF_6 are comparable to that which has been observed for **1**·I·CH_2Cl_2. The Ir center in **1**·PF_6 is coordinated by two pincer $^{nBu}(C_{NHC}{}^{Me}CC_{NHC})$ ligands, both in a *mer* arrangement, resulting in a slightly distorted octahedral coordination geometry (see Figure 2). There is a deviation

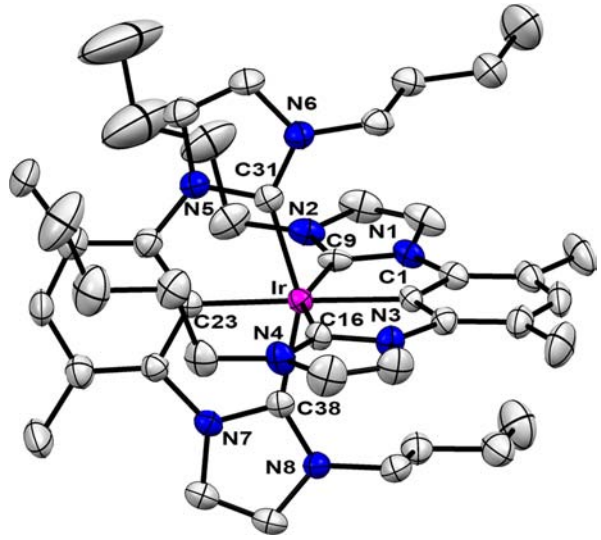

Figure 2. Perspective view of **1**·PF_6 with partial atom labeling. H atoms are omitted for clarity. Ellipsoids are represented at the 50% probability level.

from the ideal 180° of the *trans* C_{NHC}−Ir−C_{NHC} angles (C9−Ir−C16 and C31−Ir−C38 = 152.3(1)° and 153.0(1)°, respectively), resulting also in a narrowing of the C_{arom}−Ir−C_{NHC} bite angles (C_{arom}−Ir−C_{NHC} = 76.35(1)°). The average Ir−C_{NHC} distances (2.048(5) Å) well compare with the reported Ir carbene complexes.[18,41] All the most representative angles and bond lengths are collected in Table 1.

Table 1. Selected Bond Lengths and Bond Angles for Complex 1·PF_6

Bond Lengths		Bond Angles	
atom pair	[Å]	bond angle	[deg]
Ir−C9	2.05(3)	C9−Ir−C1	76.0(1)
Ir−C16	2.05(4)	C16−Ir−C1	76.3(1)
Ir−C1	2.041(3)	C31−Ir−C23	76.5(1)
Ir−C31	2.04(4)	C38−Ir−C23	76.6(1)
Ir−C38	2.05(4)	C9−Ir−C16	152.3(1)
Ir−C23	2.03(3)	C31−Ir−C38	153.0(1)
		C1−Ir−C23	178.8(1)

dx.doi.org/10.1021/ic302695q | *Inorg. Chem.* 2013, 52, 10756−10765

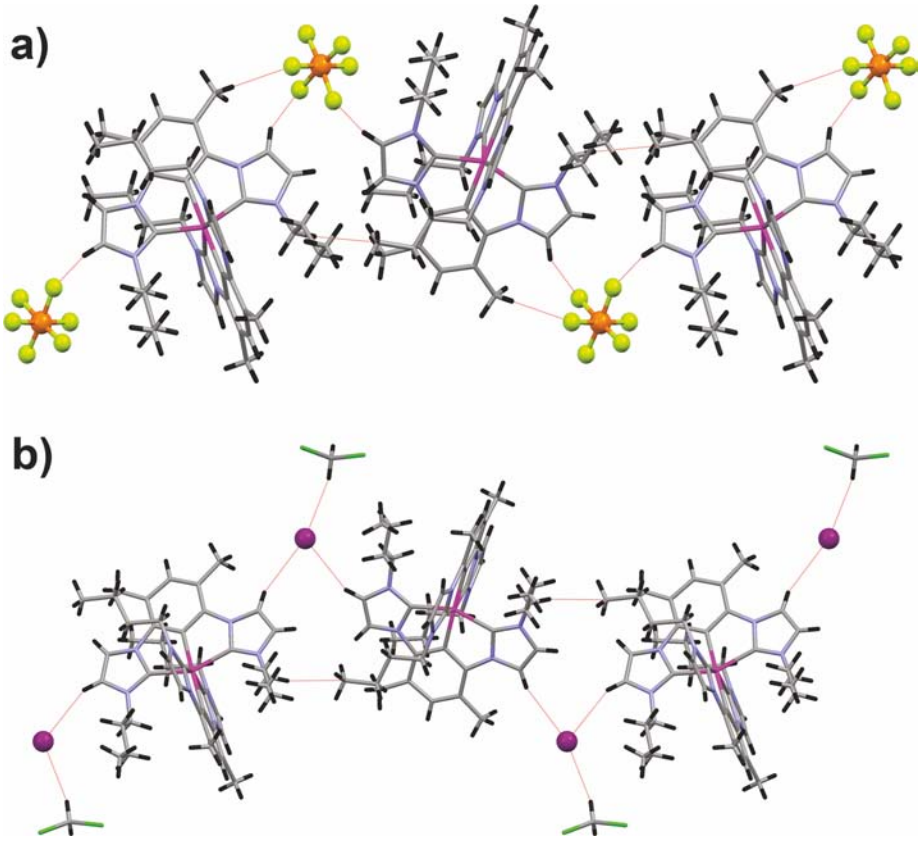

Figure 3. Perspective views of the 1D supramolecular motif along the crystallographic *a*-axis for (a) **1**·PF_6 and (b) **1**·I. C−H···X interactions are shown.

Molecular packing of **1**·I and **1**·PF_6 is primarily achieved by intermolecular interactions involving the CH group of imidazolium moiety and the counterions via nonclassical hydrogen bonding, C−H···X.[42] Along the crystallographic *a*-axis, **1**·PF_6 forms a supramolecular one-dimensional (1D) zigzag motif with the PF_6^- interacting, through the F atoms, with the CH group of the carbenes and the methyl groups of the central phenyl (Figure 3a). The average C−H···F distances is 2.596 Å. The solvated crystal structure **1**·I showed similar 1D motif along the crystallographic *a*-axis (Figure 3b), although the average distances of C−H···I interactions is significantly longer (3.115 Å) than those observed for **1**·PF_6. In addition, for the iodine derivative, the solvents organized in the structure and the length of interaction between the CH_2Cl_2 molecules and the iodine ions via C−H···I interaction is 3.030 Å. The solvent molecules are not present when the bulkier PF_6^- is used as counterion and the shorter C−H···X distances observed in **1**·PF_6 compared to **1**·I, suggesting a stronger halogen−H bond between the anions and the $^{n\mathrm{Bu}}(C_{NHC}{}^{Me}CC_{NHC})$ ligands.

Frontier Orbitals and Electrochemistry. In order to ascertain the electronic nature of the frontier orbitals of the investigated compounds, ground-state (S_0) geometrical optimization of cationic bis-pincer Ir(III) carbene complexes was performed on the closely related cationic complex $[Ir^{Me}(C_{NHC}{}^{Me}CC_{NHC})_2]^+$, **2**, where the *n*-butyl chains have been replaced by shorter methyl groups. These computed geometries have been optimized by means of density functional theory (DFT) at B3LYP/6-31G(d,p) + SDD level without any symmetry constrains (Figure 4). Starting the optimization from the structure derived from the X-ray coordinates, the lowest energy stationary point resulted to possess the highest possible

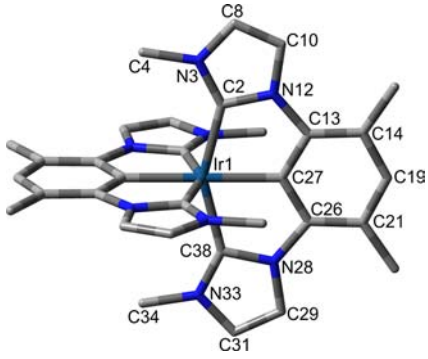

Figure 4. Optimized geometry of the complex $[Ir^{Me}(C_{NHC}{}^{Me}CC_{NHC})_2]^+$, **2**, at its ground state with partial atom labeling.

symmetry for these species as being the D_{2d} conformation. The most significant computed geometrical parameters are listed in Table S2 in the Supporting Information and nicely agree with the experimental data obtained by single-crystal X-ray diffraction. In particular, the modeled Ir−C_{ph} and Ir−C_{NHC} bonds are 2.061 (averaged experimental 2.037) and 2.084 (averaged experimental 2.050) Å, respectively.

For **2**, the energies of the orbitals closer to the frontier region are listed in Table S3 in the Supporting Information and the isodensity surface plots are depicted in Figure 5. The highest occupied molecular orbital (HOMO) lies at −7.735 eV and is the combination of Ir dπ orbitals (t_{2g}) and of phenyl π orbitals along with a noticeable contribution of the π orbital of the carbene moieties (b_1 symmetry). The lowest unoccupied

dx.doi.org/10.1021/ic302695q | *Inorg. Chem.* 2013, 52, 10756−10765

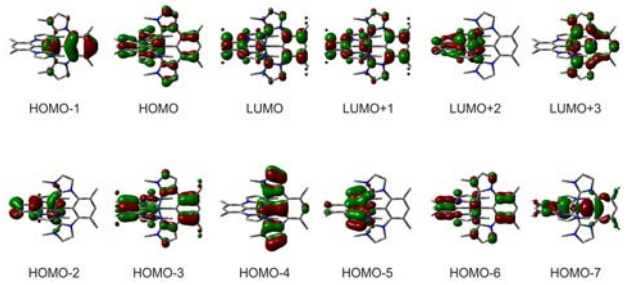

Figure 5. Isodensity surface plots of some selected frontier molecular orbitals for the complexes $[Ir^{Me}(C_{NHC}{}^{Me}CC_{NHC})_2]^+$, **2**, at its optimized S_0 geometry in the gas phase. Isodensity value 0.035 e $Bohr^{-3}$.

molecular orbital (LUMO) lies at −2.823 eV and possesses a_2 symmetry. Such a virtual orbital is the combination of the π^* orbitals of the phenyl rings with a small contribution of the π^* of the NHC moieties, while the participation of the metal orbitals is negligible.

The electrochemical behavior of the bis-pincer Ir carbene complexes was investigated by cyclic voltammetry (CV), using the redox couple ferrocinium/ferrocene ($FeCp_2^+|FeCp_2$) as the internal standard. Acetonitrile was selected as the solvent, because of the good solubility of both complexes and the large electrochemical window (exp.: +2.3 V to −2.7 V) and 0.1 M tetrabutylammonium hexafluorophosphate ($TBAPF_6$) was employed as the supporting electrolyte.

Both complexes displayed similar electrochemical profile, during anodic scan, with scan rate of 100 mV s^{-1}, oxidation peaks were observed at +0.68 V and +0.65 V vs $FeCp_2^+|FeCp_2$, for complexes **1**·I and **1**·PF_6, respectively (see Figure S1 in the Supporting Information). The peak-to-peak distance of these anodic peaks was 68 and 70 mV, for complexes **1**·I and **1**·PF_6, respectively, indicating that the anodic peaks of the complexes are reversible. These results nicely correlate with those found from reported homoleptic Ir carbene complexes.[4] The oxidation process is most likely located on the Ir metal site, together with additional contributions from the pincer carbene ligand, which is in agreement with the result observed from DFT calculation. Unfortunately, no observable reduction was detected for both complexes within the electrochemical window of acetonitrile indicating the very high reduction potential for the complexes.[4]

PHOTOPHYSICS IN SOLUTION

The absorption spectra of both cationic bis-pincer Ir-carbene complexes in CH_3CN solution (Figure 6) show a similar profile to that of neutral homoleptic Ir carbene complexes.[4] Complexes **1**·I and **1**·PF_6 exhibited an intense absorption peak at ∼270 nm (ε = 1.1−1.5 × 10^4 M^{-1} cm^{-1}) and less intense peaks of 290 and 320 nm (ε = 0.8−1.0 × 10^4 M^{-1} cm^{-1}), which were ascribed to mixed singlet manifold metal-to-ligand charge transfer and ligand centered (^{1}MLCT/^{1}LC) transitions. The highly intense absorption band in the spectral region below 250 nm (ε > 2.5 × 10^4 M^{-1} cm^{-1}) is attributed to the spin-allowed $^1\pi-\pi^*$ transition characteristic of the ligands. To gain deeper insight into the electronic properties of the transitions involved in the optical absorption processes, complex **2** was investigated by means of time-dependent DFT (TD-DFT), both in vacuum and with CH_3CN as a solvent, the latter by employing the IEFPCM solvation model.[43]

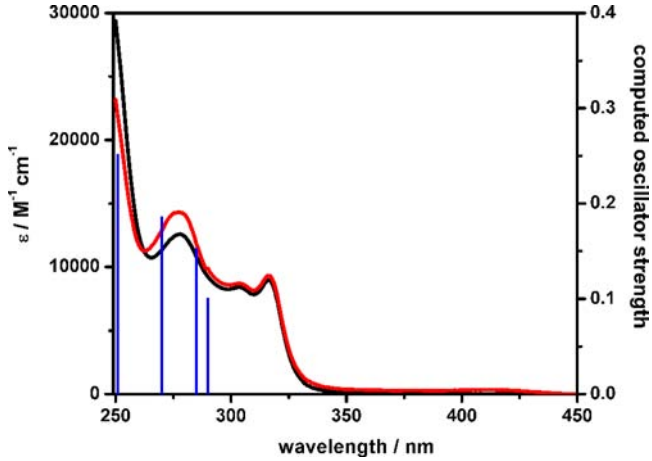

Figure 6. Absorption spectra of **1**·I (black) and **1**·PF_6 (red) in CH_3CN solution. Calculated absorption peaks (blue) of **2** in CH_3CN are shown for comparison.

The most relevant computed transitions, along with their energy, character, and oscillator strength, are listed in Table S4 in the Supporting Information. By comparison to the transitions calculated in CH_3CN, the bands around 290 nm are assigned to mixed interligand $\pi \rightarrow \pi^*$ (^{1}ILCT) and $d\pi \rightarrow \pi^*$ metal-to-ligand charge transfer (^{1}MLCT) transitions. Such findings are in nice agreement with similar compounds already reported.[4] Deconvolution of these bands results in three intense spin-allowed singlet transitions:

(i) Two intense (f = 0.101 for each of the transitions) isoenergetic absorption processes of E symmetry, corresponding to the $S_0 \rightarrow S_1$ and $S_0 \rightarrow S_2$ (HOMO−1/HOMO−2→ LUMO/LUMO+1) transitions and lying at 4.273 eV, and

(ii) An intense (f = 0.153) excitation process of $^1B_2$ symmetry corresponding to the $S_0 \rightarrow S_6$ transition (HOMO→ LUMO) and lying at 4.357 eV.

The absence of these bands in the experimental absorption spectrum of the free ligand supports their assignment as MLCT bands with strong LC contribution (see Figure S2 in the Supporting Information). No significant differences were observed in the absorption spectra of complexes with different counterions, because of the good solvation of the compounds by CH_3CN solvent molecules. It is worthy of notice that TD-DFT calculations performed in acetonitrile on the S_0 of the compound **1**·PF_6, using the geometry derived from the crystal structure and including the PF_6^- counterion (C_1 symmetry) gave very similar results, with transitions within the range of ±15 nm. The corresponding computed transitions are listed in Table S5 in the Supporting Information.

In dilute degassed (c = 1.0 × 10^{-5} M) CH_3CN solution at room temperature, the emission profiles of both complexes are identical and exhibit vibronic progression (1411 cm^{-1}) typical of emission from the ^{3}LC/^{3}MLCT excited state in tris-cyclometalated Ir complexes,[44−46] with two main emission maxima at 384 and 406 nm (Figure 7). To the best of our knowledge, this is the first example reported in the literature of Ir terdentate complexes emitting in the near-UV region. Such emission energy is in good agreement with the $S_0 \rightarrow T_1$ transition for **2** computed in acetonitrile at 370 nm (3.348 eV, $^3B_2$) by means of TD-DFT, which shows strong ^{3}LC character, as combination of phenyl(π)Ir(π)NHC(π) → phenyl(π^*)-

dx.doi.org/10.1021/ic302695q | Inorg. Chem. 2013, 52, 10756−10765

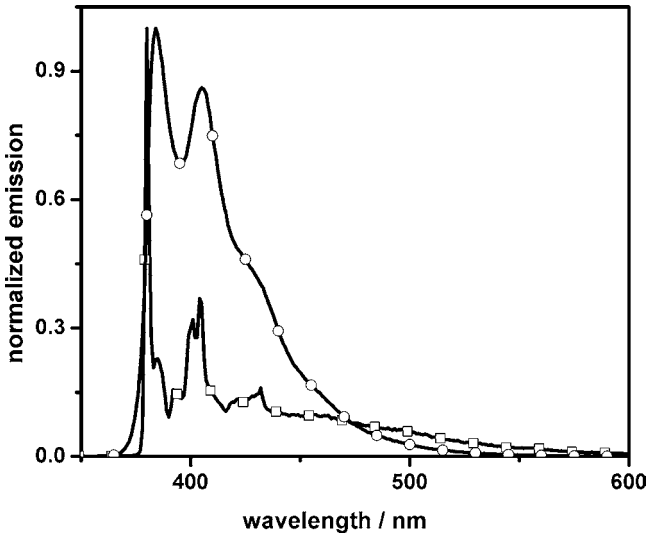

Figure 7. Emission spectra of **1**·I in degassed CH_3CN at 298 K (circle symbol, ○) and butyronitrile matrix at 77 K (square symbol, □). λ_{exc} = 315 nm. Emission spectra of **1**·I and **1**·PF_6 are superimposable.

NHC(π^*) (HOMO−3 → LUMO+1 and HOMO → LUMO excitations) (see Table S4 in the Supporting Information).

Complexes **1**·I and **1**·PF_6 exhibited high photoluminescence (PL) quantum yield (Φ) (Figure 7) of 0.41 and 0.38, respectively. The Φ value of the complexes is impressive for cationic Ir terdentate complexes in the near-UV region,[21] thus highlights the mutual benefits in the introduction of such strong field ligands, for the emission color tuning to the blue region, and improvement of photoluminescence efficiency in the more-rigid Ir terdentate systems. Under deaerated conditions, the luminescence decays show similar excited state lifetimes: 8.9 and 9.4 μs for complexes **1**·I and **1**·PF_6, respectively (Table 2). The long excited-state lifetimes and the structured emission profile corroborate the idea that the excited states of bis-pincer Ir carbene complexes are admixtures of ^{3}MLCT and ^{3}LC states. In addition, the calculated values of the radiative (k_r) and nonradiative (k_{nr}) rate constants are also very similar for both complexes (Table 2). When going from room temperature to a butyronitrile glassy matrix at 77 K, the spectra exhibit highly structured profile and a 274 cm^{-1} hypsochromic shift with longer lifetimes of 15.7 and 15.2 μs, for complexes **1**·I and **1**·PF_6, respectively, suggesting more ligand-centered excited states. Indeed, the lack of solvent stabilization in the rigid frozen matrix causes a shift to higher energy of the MLCT states, resulting in a lower degree of level of mixing.

■ PHOTOPHYSICS IN SOLID STATE

The photophysical behavior of the complexes in solid state has been investigated, and interesting differences have been observed, compared to the solution. Crystals of **1**·I exhibit a large red shift of the emission (116 nm, 6042 cm^{-1}) with respect to the solution, with emission maxima at 500 nm (see Figure 8). The emission profile is broad and featureless, with a significant decrease in the excited-state lifetime and the Φ value (see Table 2). Interestingly, crystals of **1**·PF_6 showed two emission bands. The original high-energy emission is similar to that observed in solution, with maxima at 384 and 406 nm, and a concomitant new low-energy emission is identical to that of the crystalline **1**·I (see Figure 8). We also observe that the emission decay for crystal **1**·PF_6 is longer than that for crystal **1**·

Table 2. Photophysical Properties of the Complexes 1·I and 1·PF_6 in Degassed CH_3CN at Room Temperature, Butyronitrile Glass Matrix at 77 K, and as Crystalline Solids

medium	temperature [K]	λ_{abs} [nm] (ε [$\times 10^{-4}$ M^{-1} cm^{-1}])	λ_{em}[a,b] [nm]	PLQY[b]	τ_{obs} [μs]	k_r [$\times 10^{-4}$ s^{-1}]	k_{nr} [$\times 10^{-4}$ s^{-1}]
			Complex **1**·I				
CH_3CN	298	270 (1.2), 290 (0.8), 320 (0.9), 335 (0.08)	384, 406, 430 (sh)	0.41	8.9[c]	4.6	6.6
butyronitrile	77		380, 406, 410, 430 (sh)		15.7[c]		
crystal	298		500	0.12	1.0 (45%), 4.7 (55%)[d]	3.9	28.9
			Complex **1**·PF_6				
CH_3CN	298	270 (1.4), 290 (0.8), 320 (0.9), 335 (0.08)	384, 406	0.38	9.4[c]	4.1	6.5
butyronitrile	77		380, 406, 410, 430 (sh)		15.2[c]		
crystal	298		384, 406, 430 (sh), 500	0.20	1.8 (50%), 6.8 (50%)[d]	4.6	18.6

[a]"sh" denotes a shoulder. [b]λ_{exc} = 315 nm. [c]Monitored at λ_{em} = 384 nm. [d]Monitored at λ_{em} = 500 nm.

dx.doi.org/10.1021/ic302695q | Inorg. Chem. 2013, 52, 10756−10765

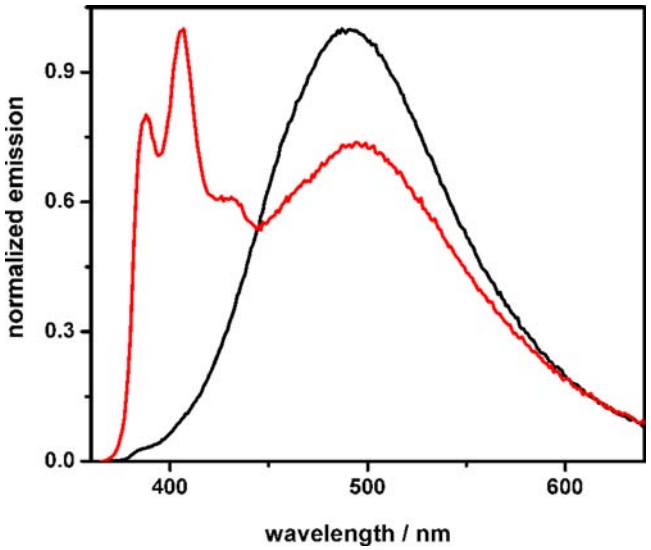

Figure 8. Emission spectra of **1**·I (black) and **1**·PF_6 (red) in crystalline state. λ_{exc} = 315 nm.

I, suggesting that the excited states are more quenched in the latter case. The Φ value for the crystalline **1**·PF_6 is almost twice higher than **1**·I, with values of 0.2 and 0.12, respectively.

The origin of the new low-energy emissions in the **1**·I and **1**·PF_6 crystals could be caused by different factors related to aggregation, defects, and charge-transfer processes. We can exclude charge-transfer phenomena where the different counterions are involved, since different emission energy should be observed when going from PF_6^- to I^-. The formation of excimers or aggregates[47] has been excluded in solution by measuring the absorption and emission spectra in a very large concentration range, from 5.0×10^{-6} to 1.0×10^{-3} M in acetonitrile (see Figures S3 and S4 in the Supporting Information). No changes in the profile and maxima of the spectra have been observed. In the solid state, dimer formation[48] is not likely to be responsible for the red-shift emission, because of the fact that, from X-ray analysis, there are no strong couplings of any type between the molecules. Also, the influence of the solvent molecules inside the crystals that contain I^- as a counterion is not likely to play a major role; however, it would allow a more flexible and easily packing of the complexes.

Therefore, we believe that the different photophysical properties for the **1**·I and **1**·PF_6 crystals are due to the formation of new trapping species present when the more-polarizable iodine is used as a counterion. A local aggregation of the complexes can occur in the **1**·I complex, which is much less pronounced in the stiffer hexafluorophosphate complex. Indeed, X-ray analysis showed that the counterions act as connecting units between the cationic emitter via C−H···X interactions, with the distance of C−H···F and C−H···I being 2.596 and 3.115 Å, respectively. Consequently, the interactions are smaller in the case of **1**·I, relative to **1**·PF_6, favoring the formation of the trapping sites. A similar red-shift emission has been recently reported for crystalline cationic Ir complexes containing picolylamine ligand with different counterion molecules.[49]

To confirm this aggregation hypothesis, in the solid state, concentration-dependent emission study was performed in amorphous PMMA thin films doped with increasing concentration of the complexes. Increasing the concentration of the complex in the solid matrix should increase the probability to form trapping species and therefore allow the formation of the low-energy emission states. Indeed, as shown in Figure 9, at doping concentrations below 25%, the emission spectra are similar to those obtained in acetonitrile solutions. When the doping concentrations are increased, the relative intensity of the low-energy emission at ∼500 nm increases and the ratio between the low- and high-energy emission changes, depending on the counterion of the complex investigated. In general, the excited-state lifetimes and emission quantum yields of the thin films decrease by increasing the doping concentration (see Table 3).

Also, in the amorphous films, the influence of the iodine versus the hexafluorophosphate is remarkable. The comparison clearly shows that the red emission is very pronounced for **1**·I already at a doping concentration of 50%, accompanied by a decrease in the excited-state lifetime and Φ (see Table 3). At the same concentration, **1**·PF_6 shows only a minor band formed at ∼500 nm. In neat film (100 wt %), the ratio between the two emission bands is completely different for the two complexes (see Figure 9).

PRELIMINARY DEVICE

As a proof of principle, we successfully fabricated electroluminescent devices by spin-coating **1**·PF_6 and PMMA (1:1) from a chlorobenzene solution. The device configuration is

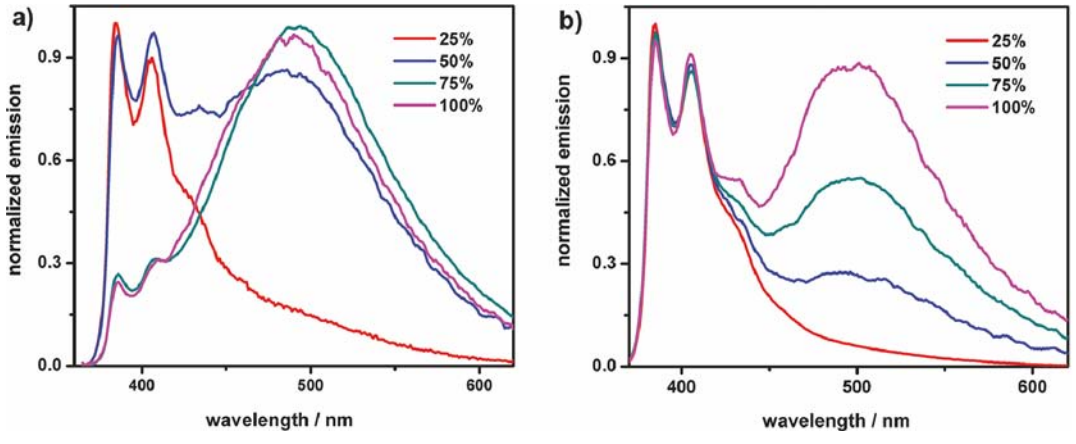

Figure 9. Emission spectra of (a) **1**·I and (b) **1**·PF_6 in PMMA in weight percentage. 100% means neat film. λ_{exc} = 315 nm.

dx.doi.org/10.1021/ic302695q | Inorg. Chem. 2013, 52, 10756−10765

Table 3. Photophysical Properties of the 1·I and 1·PF_6 Complexes in PMMA Thin Films with Various Doping Concentrations

doping concentration (%)	1·I			1·PF_6		
	RI[a]	τ_{obs} [μs][b]	Φ[c]	RI[a]	τ_{obs} [μs][b]	Φ[c]
5	20	6.5	0.30	23	9.1	0.40
10	16	1.9 (43%), 4.5 (57%)	0.10	19.2	9.0	0.36
25	6.6	0.85 (32%), 4.0 (68%)	0.09	13.8	5.9	0.25
50	1.2	0.85 (49%), 3.9 (51%)	0.07	3.7	1.4 (49%), 4.6 (51%)	0.10
75	0.2	0.70(65%), 3.6 (35%)	0.04	1.9	0.85 (45%), 4.0 (55%)	0.07
100	0.2	0.70 (68%), 3.5 (32%)	0.03	1.1	0.85 (52%), 4.1 (48%)	0.05

[a]RI denotes as ratio intensity of emission between high-energy emission (384 nm) and low-energy emission (500 nm). [b]Monitored at λ_{em} = 384 nm. [c]λ_{exc} = 315 nm.

depicted in Figure S5 in the Supporting Information. Although the efficiency of an unoptimized device is very low (<1%), the electroluminescence in the near-UV region of the spectrum with maxima at 386 and 406 nm could be observed (see Figure 10a). These peaks correspond well to the PL peaks measured in solution, as well as in PMMA (Figure 9b). The turn-on voltage is ~8 V, as shown by the current−voltage (I−V) curve (Figure 10b).

CONCLUSION

We have synthesized and studied the photophysical properties of cationic bis-pincer Ir(III) complexes **1**·I and **1**·PF_6. The compounds have an intense emission in the near-UV region and interesting emission quantum yields of 0.41 and 0.38, respectively. The nature of the lowest luminescent excited state, an admixed ^{3}MLCT and ^{3}LC level, was also confirmed by DFT calculation. Surprisingly, in the solid state, the emission exhibited peculiar behavior, depending on the counterion that was employed. We observed a concentration-dependent energy emission at ~500 nm that we attributed to the formation of trapping species. The dual emission can be further exploited to build up electroluminescent devices with broad emission in order to obtain white light in a single component. The first near-UV electroluminescent device based on charged iridium complexes has been constructed to show the potential of the approach.

EXPERIMENTAL SECTION

Synthesis and Characterization. All the reactions were carried out under inert atmosphere (via the Schlenk technique). All the solvents were used as-received from Aldrich or Fluka, without any further purification. All the chemicals were purchased and used as-received. ^{1}H NMR spectra were recorded on an ARX 300 system (Bruker Analytische Messtechnik, Karlsruhe, Germany) at 300 K. The ^{1}H NMR chemical shifts (δ) are given in ppm and referred to residual protons on the corresponding deuterated solvent. All deuterated solvents were used as received without any further purification. All coupling constants (J) are given in Hertz (Hz). Mass spectrometry was performed at the Department of Organic Chemistry, University of Münster (Germany). Electrospray ionization (ESI) mass spectra were recorded on a Bruker Daltonics MicroTof with loop injection (Bremen, Germany). Elemental analyses were performed on a Perkin−Elmer CHN2400 instrument at the University of Milan (Italy).

Synthesis of 1·I (Bis{(4,6-dimethyl-1,3-phenylene-κC^2)bis(1-butylimidazol-2-ylidene)} iridium(III) Iodide). The complex was prepared according to previous reports with 65% yield.[41] ^{1}H NMR (CD_3CN): δ 7.94 (d, $^3J_{(HH)}$ = 2.1 Hz, 4H), 6.92 (s, 2H), 6.86 (d, $^3J_{(HH)}$ = 2.1 Hz, 4H), 2.83 (m, 8H), 2.72 (s, 12H), 0.64 (br s, 28H). HRMS (ESI): $[M - I]^+$ 891.4627, calcd for $C_{44}H_{58}IrN_8$ 891.4390. Anal. Calcd for $C_{44}H_{58}IIrN_8 \times 3CH_2Cl_2$ (1103.04): C, 49.00; H, 5.48; N, 10.16. Found: C, 49.15; H, 5.47; N, 10.29.

Synthesis of 1·PF_6 (Bis{(4,6-dimethyl-1,3-phenylene-κC^2)bis(1-butylimidazol-2-ylidene)}iridium(III) hexafluorophosphate). Complex **1**·I (0.5 g, 0.49 mmol) was dissolved in the mixture of CH_2Cl_2/MeOH (2:1, 20 mL) and NH_4PF_6 (0.4 g, 2.4 mmol)/MeOH (5 mL) was added into the solution. The mixture was stirred at room temperature for 12 h. The solvent was removed in vacuo and residue was washed with deionized water (40 mL). The residue was purified by column chromatography (CH_2Cl_2/CH_3CN, 1:1) and recrystallization from CH_2Cl_2/Et_2O gave **1**·PF_6 as an off-white solid in quantitative yield. ^{1}H NMR (300 MHz, CD_2Cl_2) δ 7.84 (d, J = 2.2 Hz, 4H), 6.90 (s, 2H), 6.71 (d, J = 2.2 Hz, 4H), 2.86 (m, 8H), 2.73 (s, 12H), 0.62 (m, 28H). HR-MS (ESI) ($[M-PF_6]^+$) 891.4430 calcd for $C_{44}H_{58}IrN_8$ 891.4390; Anal. Calcd for

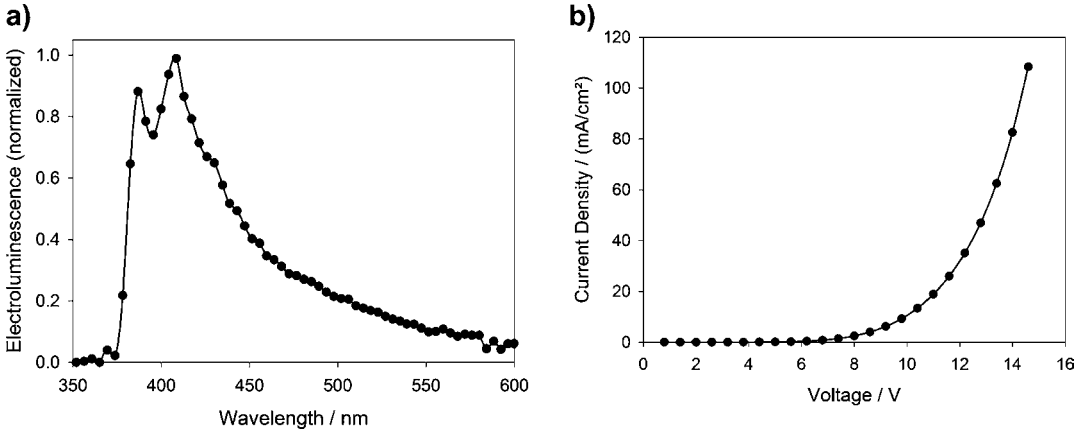

Figure 10. (a) Electroluminescence (EL) spectrum of **1**·PF_6 (50 wt % in PMMA). (b) I−V curve.

dx.doi.org/10.1021/ic302695q | Inorg. Chem. 2013, 52, 10756−10765

$C_{44}H_{58}IrN_8PF_6$ (1036.16): C, 51.00; H, 5.64; N, 10.81. Found: C, 51.30; H, 5.56; N, 10.97.

X-ray Data Collection, Structure Solution, and Refinement. The intensity data were collected at 173(2) K on a Kappa CCD diffractometer (graphite-monochromated Mo Kα radiation, λ = 0.71073 Å).[50] Crystallographic and experimental details for the structures are summarized in Table S1 in the Supporting Information. The structures were solved by direct methods (SHELXS-97)[51] and refined by full-matrix least-squares procedures (based on F^2, SHELXL- 97) with anisotropic thermal parameters for all the non-hydrogen atoms. The hydrogen atoms were introduced into the geometrically calculated positions (SHELXL-97 procedures) and refined riding on the corresponding parent atoms.

Photophysical Measurements. Absorption spectra were measured on a Varian Cary 5000 double-beam UV−vis spectrometer and baseline-corrected. Steady-state emission spectra were recorded on a Horiba Jobin−Yvon IBH FL-322 Fluorolog 3 spectrometer equipped with a 450-W xenon arc lamp, double-grating excitation, and emission monochromators (2.1 nm mm^{-1} of dispersion; 1200 grooves mm^{-1}) and a Hamamatsu R928 photomultiplier tube or a TBX-4-X single-photon-counting detector. Emission and excitation spectra were corrected for source intensity (lamp and grating) and emission spectral response (detector and grating) by standard correction curves. Time-resolved measurements were performed using the time-correlated single-photon-counting option on the Fluorolog 3. NanoLEDs (295 nm; full width at half maximum (fwhm) < 1 ns) with repetition rates between 10 kHz and 1 MHz were used to excite the sample. The excitation sources were mounted directly on the sample chamber at 90° to a double-grating emission monochromator (2.1 nm mm^{-1} of dispersion; 1200 grooves mm^{-1}) and collected by a TBX-4-X single-photon-counting detector. The photons collected at the detector are correlated by a time-to-amplitude converter to the excitation pulse. Signals were collected using an IBH DataStation Hub photon-counting module, and data analysis was performed using the commercially available DAS6 software (Horiba Jobin−Yvon IBH). The quality of the fit was assessed by minimizing the reduced χ^2 function and visual inspection of the weighted residuals. The quantum yield measurements were performed in an acetonitrile solution at an excitation wavelength of 315 nm using an absolute quantum yield measurement system (Hamamatsu, Model C9920-01).

Cyclic Voltammetry (CV). CV measurements were performed using a CH Instrument workstation, which consists of a CH750 potentiostat and software. The working electrodes and counterelectrodes were a platinum disk and a platinum wire, respectively, whereas a silver wire was used as the pseudo-reference electrode. All glassware was dried prior to use. The dry electrolyte tetrabutylammonium hexafluorophosphate was used after recrystallization. The analyte and ferrocene ($FeCp_2$) used as the reference were dried and degassed at high temperature and at reduced pressure in a Schlenk flask, in order to eliminate any moisture and oxygen. The flask was then evacuated and filled three times with a nitrogen flow. Acetonitrile freshly distilled from P_2O_5 was added via syringe directly into the sealed Schlenk flask; the solution was sonicated if necessary and then degassed for 10 min with a gentle stream of nitrogen. The degassed solution was injected into the electrochemical cell, and after the introduction of electrodes, measurements were performed under a nitrogen atmosphere.

Computational Methods. Geometries were optimized by means of density functional theory (DFT), employing the exchange correlation hybrid functional B3LYP.[52−54] The standard valence double-ζ polarized basis set 6-31G(d,p)[55] was used for C, H, N, F, and P for ground-state (S_0) optimizations. For Ir, the Stuttgart−Dresden (SDD) effective core potential was employed, along with the corresponding valence triple-ζ basis set. The nature of all of the stationary points was checked by computing vibrational frequencies, and all of the species were determined to be true potential energy minima, since no imaginary frequency was obtained (NImag = 0). In order to simulate the absorption electronic spectrum down to ~250 nm, the lowest 30 singlet excitation energies ($S_0 \rightarrow S_n$, n = 1−30), as well as the five lowest triplet excitation energies ($S_0 \rightarrow T_m$, m = 1−5) were computed on the optimized geometry at the S_0 state by means of time-dependent density functional calculations (TD-DFT), at the same level of accuracy of the ground state.[56−58] Oscillator strengths were deduced from the dipole transition-matrix elements (for single states only). All these calculations were performed under vacuum. TD-DFT calculations were also performed on the gas-phase S_0 optimized geometry in the presence of acetonitrile as the solvent, as described by the IEFPCM. All the calculations were performed with Gaussian 09W program package.[59]

Electroluminescent Device. The device using **1**·PF_6 as an emitter was prepared as follows. The indium tin oxide (ITO)-coated glass substrate was cleaned and treated for 15 min with UV/O_3 at room temperature. An 80-nm PEDOT:PSS-layer (Heraeus PVP 4083 AI) was deposited on top of the ITO by spin-coating and then annealed at 180 °C for 10 min to remove residual water. An 80-nm emissive layer was spin-coated from a chlorobenzene solution of **1**·PF_6 (50 wt %) in PMMA (Sigma−Aldrich), which was filtered through a polytetrafluoroethylene (PTFE) filter (Millipore Millex LS; 5 μm) prior to spin-coating. The device was then heat-treated at 80 °C for 10 min. One hundred nanometers (100 nm) of aluminum was evaporated as the top electrode. The device was then encapsulated and characterized.

■ ASSOCIATED CONTENT

Supporting Information

X-ray crystallographic data file (CIF) for complex **1**·PF_6. Crystal data and structure refinement parameters for complex **1**·PF_6. Geometrical parameters and energy of selected molecular orbital. Cyclic voltammograms of complexes **1**·I and **1**·PF_6 recorded in acetonitrile. Absorption spectrum of free ligand. Concentration-dependent absorption and emission spectra of **1**·I. Schematic view of the near-UV electroluminescent device. This material is available free of charge via the Internet at http://pubs.acs.org.

■ AUTHOR INFORMATION

Corresponding Author

*E-mail: decola@unistra.fr.

Present Address

[⊥]Institut de Science et d'Ingénierie Supramoléculaires, UMR 7006, Université de Strasbourg, 8 allée Gaspard Monge, F-67083 Strasbourg, France.

Notes

The authors declare no competing financial interest.

■ ACKNOWLEDGMENTS

N.D. thanks the NRW Graduate School, University of Muenster for financial support. M.M. thanks Alexander von Humboldt Foundation for the fellowship and Université de Strasbourg. L.D.C. thanks Axa Research Fund and Gutenberg Chair. P.B. thanks the CNRS, the Ministère de la Recherche and IFP energies nouvelles for funding.

■ REFERENCES

(1) Yersin, H. *Highly Efficient OLEDs with Phosphorescent Materials*; Wiley−VCH Verlag GmbH & Co. KGaA: Weinheim, Germany, 2008.
(2) Baldo, M. A.; O'Brien, D. F.; You, Y.; Shoustikov, A.; Sibley, S.; Thompson, M. E.; Forrest, S. R. *Nature* **1998**, *395*, 151−154.
(3) Fu, H.; Cheng, Y. M.; Chou, P. T.; Chi, Y. *Mater. Today* **2011**, *14*, 472−479.
(4) Sajoto, T.; Djurovich, P. I.; Tamayo, A.; Yousufuddin, M.; Bau, R.; Thompson, M. E.; Holmes, R. J.; Forrest, S. R. *Inorg. Chem.* **2005**, *44*, 7992−8003.
(5) Holmes, R. J.; Forrest, S. R.; Sajoto, T.; Tamayo, A.; Djurovich, P. I.; Thompson, M. E.; Brooks, J.; Tung, Y. J.; D'Andrade, B. W.; Weaver, M. S.; Kwong, R. C.; Brown, J. J. *Appl. Phys. Lett.* **2005**, *87*, 243507−243509.
(6) Sajoto, T.; Djurovich, P. I.; Tamayo, A. B.; Oxgaard, J.; Goddard, W. A., III; Thompson, M. E. *J. Am. Chem. Soc.* **2009**, *131*, 9813−9822.
(7) Jeon, S. O.; Jang, S. E.; Son, H. S.; Lee, J. Y. *Adv. Mater.* **2011**, *23*, 1436−1441.
(8) Yang, C.-H.; Cheng, Y.-M.; Chi, Y.; Hsu, C.-J.; Fang, F.-C.; Wong, K.-T.; Chou, P.-T.; Chang, C.-H.; Tsai, M.-H.; Wu, C.-C. *Angew. Chem., Int. Ed.* **2007**, *46*, 2418−2421.
(9) Chang, C.-F.; Cheng, Y.-M.; Chi, Y.; Chiu, Y.-C.; Lin, C.-C.; Lee, G.-H.; Chou, P.-T.; Chen, C.-C.; Chang, C.-H.; Wu, C.-C. *Angew. Chem., Int. Ed.* **2008**, *47*, 4542−4545.
(10) Mercs, L.; Albrecht, M. *Chem. Soc. Rev.* **2010**, *93*, 1903−1912.
(11) Slinker, J.; Bernards, D.; Houston, P. L.; Abruña, H. D.; Bernhard, S.; Malliaras, G. G. *Chem. Commun.* **2003**, *9*, 2392−2399.
(12) Slinker, J. D.; Rivnay, J.; Moskowitz, J. S.; Parker, J. B.; Bernhard, S.; Abruna, H. D.; Malliaras, G. G. *J. Mater. Chem.* **2007**, *17*, 2976−2988.
(13) Costa, R. D.; Ortí, E.; Bolink, H. J. *Pure Appl. Chem.* **2011**, *83*, 2115−2128.
(14) Costa, R. D.; Ortí, E.; Bolink, H. J.; Monti, F.; Accorsi, G.; Armaroli, N. *Angew. Chem., Int. Ed.* **2012**, *51*, 8178−8211.
(15) Lim, S. *J. Soc. Inf. Display* **2011**, *19*, 882−887.
(16) Hönigsmann, H. *Semin. Dermatol.* **1990**, *9*, 84−90.
(17) Hönigsmann, H. *Clin. Exp. Dermatol.* **2001**, *26*, 343−350.
(18) Yang, C.-H.; Beltran, J.; Lemaur, V.; Cornil, J.; Hartmann, D.; Sarfert, W.; Fröhlich, R.; Bizzarri, C.; De Cola, L. *Inorg. Chem.* **2010**, *49*, 9891−9901.
(19) Lu, K. Y.; Chou, H. H.; Hsieh, C. H.; Yang, Y. H. O.; Tsai, H. R.; Tsai, H. Y.; Hsu, L. C.; Chen, C. Y.; Chen, I. C.; Cheng, C. H. *Adv. Mater.* **2011**, *23*, 4933−4937.
(20) Kessler, F.; Costa, R. D.; Di Censo, D.; Scopelliti, R.; Ortí, E.; Bolink, H. J.; Meier, S.; Sarfert, W.; Grätzel, M.; Nazeeruddin, M. K.; Baranoff, E. *Dalton Trans.* **2012**, *41*, 180−191.
(21) Williams, J. A. G.; Wilkinson, A. J.; Whittle, V. L. *Dalton Trans.* **2008**, 2081−2099.
(22) Williams, J. A. G. *Chem. Soc. Rev.* **2009**, *38*, 1783−1801.
(23) Wilkinson, A. J.; Goeta, A. E.; Foster, C. E.; Williams, J. A. G. *Inorg. Chem.* **2004**, *43*, 6513−6515.
(24) Obara, S.; Itabashi, M.; Okuda, F.; Tamaki, S.; Tanabe, Y.; Ishii, Y.; Nozaki, K.; Haga, M. A. *Inorg. Chem.* **2006**, *45*, 8907−8921.
(25) Brulatti, P.; Gildea, R. J.; Howard, J. A. K.; Fattori, V.; Cocchi, M.; Williams, J. A. G. *Inorg. Chem.* **2012**, *51*, 3813−3826.
(26) Peris, E.; Loch, J. A.; Mata, J.; Crabtree, R. H. *Chem. Commun.* **2001**, 201−202.
(27) Loch, J. A.; Albrecht, M.; Peris, E.; Mata, J.; Faller, J. W.; Crabtree, R. H. *Organometallics* **2002**, *21*, 700−706.
(28) Tulloch, A. A. D.; Danopoulos, A. A.; Tizzard, G. J.; Coles, S. J.; Hursthouse, M. B.; Hay-Motherwell, R. S.; Motherwell, W. B. *Chem. Commun.* **2001**, 1270−1271.
(29) Cho, J.; Hollis, T. K.; Helgert, T. R.; Valente, E. J. *Chem. Commun.* **2008**, 5001−5003.
(30) Lv, K.; Cui, D. *Organometallics* **2008**, *27*, 5438−5440.
(31) Chung, L.-H.; Chan, S.-C.; Lee, W.-C.; Wong, C.-Y. *Inorg. Chem.* **2012**, *51*, 8693−8703.
(32) Helgert, T. R.; Hollis, T. K.; Valente, E. J. *Organometallics* **2012**, *31*, 3002−3009.
(33) Zhang, X.; Wright, A. M.; Deyonker, N. J.; Hollis, T. K.; Hammer, N. I.; Webster, C. E.; Valente, E. J. *Organometallics* **2012**, *31*, 1664−1672.
(34) Fleetham, T.; Wang, Z.; Li, J. *Org. Electron.* **2012**, *13*, 1430−1435.
(35) Chianese, A. R.; Mo, A.; Lampland, N. L.; Swartz, R. L.; Bremer, P. T. *Organometallics* **2010**, *29*, 3019−3026.
(36) Chianese, A. R.; Shaner, S. E.; Tendler, J. A.; Pudalov, D. M.; Shopov, D. Y.; Kim, D.; Rogers, S. L.; Mo, A. *Organometallics* **2012**, *31*, 7359−7367.
(37) Raynal, M.; Cazin, C. S. J.; Vallee, C.; Olivier-Bourbigou, H.; Braunstein, P. *Chem. Commun.* **2008**, 3983−3985.
(38) Zuo, W.; Braunstein, P. *Organometallics* **2012**, *31*, 2606−2615.
(39) Zuo, W.; Braunstein, P. *Dalton Trans.* **2012**, *41*, 636−643.
(40) Majima, K.; Watanabe, M.; Okuda, F.; Haga, M.; Yang, L. (Idemitsu Kosan Co., Ltd., Japan; Chuo University). Jpn. Patent No. JP2008266163 (A), 2008.
(41) Raynal, M.; Liu, X.; Pattacini, R.; Vallée, C.; Olivier-Bourbigou, H.; Braunstein, P. *Dalton Trans.* **2009**, 7288−7293.
(42) Rit, A.; Pape, T.; Hahn, F. E. *Organometallics* **2011**, *30*, 6393−6401.
(43) Scalmani, G.; Frisch, M. J. *J. Chem. Phys.* **2010**, *132*, 114110−114115.
(44) Lamansky, S.; Djurovich, P.; Murphy, D.; Abdel-Razzaq, F.; Kwong, R.; Tsyba, I.; Bortz, M.; Mui, B.; Bau, R.; Thompson, M. E. *Inorg. Chem.* **2001**, *40*, 1704−1711.
(45) Lamansky, S.; Djurovich, P.; Murphy, D.; Abdel-Razzaq, F.; Lee, H. E.; Adachi, C.; Burrows, P. E.; Forrest, S. R.; Thompson, M. E. *J. Am. Chem. Soc.* **2001**, *123*, 4304−4312.
(46) Tamayo, A. B.; Alleyne, B. D.; Djurovich, P. I.; Lamansky, S.; Tsyba, I.; Ho, N. N.; Bau, R.; Thompson, M. E. *J. Am. Chem. Soc.* **2003**, *125*, 7377−7387.
(47) Birks, J. B. *Rep. Prog. Phys.* **1975**, *38*, 903−974.
(48) Bolink, H. J.; Cappelli, L.; Cheylan, S.; Coronado, E.; Costa, R. D.; Lardiés, N.; Nazeeruddin, M. K.; Ortí, E. *J. Mater. Chem.* **2007**, *17*, 5032−5041.
(49) Mastropietro, T.; Yadav, Y.; Szerb, E.; Talarico, A.; Ghedini, M.; Crispini, A. *Dalton Trans.* **2012**, *41*, 8899−8907.
(50) Bruker-Nonius. *Kappa CCD Reference Manual*; Nonius BV: The Netherlands, 1998.
(51) Sheldrick, G. M. *SHELXL-97*, 1997.
(52) Lee, C.; Yang, W.; Parr, R. G. *Phys. Rev. B* **1988**, *37*, 785−789.
(53) Becke, A. D. *J. Chem. Phys.* **1993**, *98*, 5648−5652.
(54) Hay, P. J. *J. Chem. Phys. A* **2002**, *106*, 1634−1641.
(55) Francl, M. M.; Pietro, W. J.; Hehre, W. J.; Binkley, J. S.; Gordon, M. S.; DeFrees, D. J.; Pople, J. A. *J. Chem. Phys.* **1982**, *77*, 3654−3665.
(56) Stratmann, R. E.; Scuseria, G. E.; Frisch, M. J. *J. Chem. Phys.* **1998**, *109*, 8218−8224.
(57) Casida, M. E.; Jamorski, C.; Casida, K. C.; Salahub, D. R. *J. Chem. Phys.* **1998**, *108*, 4439−4449.
(58) Casida, M. E.; Huix-Rotllant, M. *Annu. Rev. Phys. Chem.* **2012**, *63*, 287−323.
(59) Frisch, M. J.; Trucks, G. W.; Schlegel, H. B.; Scuseria, G. E.; Robb, M. A.; Cheeseman, J. R.; Montgomery, Jr., J. A.; Vreven, T.; Kudin, K. N.; Burant, J. C.; Millam, J. M.; Iyengar, S. S.; Tomasi, J.; Barone, V.; Mennucci, B.; Cossi, M.; Scalmani, G.; Rega, N.; Petersson, G. A.; Nakatsuji, H.; Hada, M.; Ehara, M.; Toyota, K.; Fukuda, R.; Hasegawa, J.; Ishida, M.; Nakajima, T.; Honda, Y.; Kitao, O.; Nakai, H.; Klene, M.; Li, X.; Knox, J. E.; Hratchian, H. P.; Cross, J.

B.; Bakken, V.; Adamo, C.; Jaramillo, J.; Gomperts, R.; Stratmann, R. E.; Yazyev, O.; Austin, A. J.; Cammi, R.; Pomelli, C.; Ochterski, J. W.; Ayala, P. Y.; Morokuma, K.; Voth, G. A.; Salvador, P.; Dannenberg, J. J. *Gaussian 09*, Revision B.01; Gaussian: Wallingford, CT, 2010.